Journal of Materials Chemistry C

RSC Publishing

PAPER

View Article Online
View Journal | View Issue

Cite this: J. Mater. Chem. C, 2013, 1, 5747

Confined organization of fullerene units along high polymer chains†

Lei Fang,[a] Peng Liu,[b] Benjamin R. Sveinbjornsson,[c] Sule Atahan-Evrenk,[d] Koen Vandewal,[e] Sílvia Osuna,[b] Gonzalo Jiménez-Osés,[b] Supriya Shrestha,[d] Gaurav Giri,[a] Peng Wei,[a] Alberto Salleo,[e] Alán Aspuru-Guzik,[d] Robert H. Grubbs,[c] K. N. Houk[b] and Zhenan Bao*[a]

Received 16th June 2013
Accepted 15th July 2013

DOI: 10.1039/c3tc31158a

www.rsc.org/MaterialsC

Conductive fullerene (C_{60}) units were designed to be arranged in one dimensional close contact by locally organizing them with covalent bonds in a spatially constrained manner. Combined molecular dynamics and quantum chemical calculations predicted that the intramolecular electronic interactions (*i.e.* charge transport) between the pendant C_{60} units could be controlled by the length of the spacers linking the C_{60} units and the polymer main chain. In this context, C_{60} side-chain polymers with high relative degrees of polymerization up to 1220 and fullerene compositions up to 53% were synthesized by ruthenium catalyzed ring-opening metathesis polymerization of the corresponding norbornene-functionalized monomers. UV/vis absorption and photothermal deflection spectra corroborated the enhanced inter-fullerene interactions along the polymer chains. The electron mobility measured for the thin film field-effect transistor devices from the polymers was more than an order of magnitude higher than that from the monomers, as a result of the stronger electronic coupling between the adjacent fullerene units within the long polymer chains. This molecular design strategy represents a general approach to the enhancement of charge transport properties of organic materials *via* covalent bond-based organization.

1 Introduction

The electronic and optoelectronic properties of organic semiconductors depend heavily on non-covalent intermolecular interactions, which result in specific molecular arrangements, crystal packing modes, and morphology in the solid state. Good carrier mobility of an organic field-effect transistor (OFET), for example, can only be achieved[1] when the molecular packing mode favors maximized electronic coupling between adjacent molecules. In this context, the knowledge of crystal engineering[2–4] and supramolecular chemistry[5,6] has been applied extensively in order to gain a better understanding of the correlation between molecular structure, solid-state arrangement, and electronic/optoelectronic properties. However, it is still a challenge to control the intermolecular order in the solid state, which can be determined by many different factors such as packing enthalpy and entropy, crystallization kinetics, and metastable states.

One way to avoid the unpredictability of non-covalent intermolecular interactions in organic semiconductors is to fix the conductive components using covalent bonds. In such a case, the local arrangement of these components becomes an *intramolecular* property that is governed by the chemical constitution of covalent bonds, which is less sensitive to the possible thermal fluctuation or crystallization kinetics. For example, DNA represents a prototype model in which long-range charge transport along the π-stacked base pairs can be promoted by the special arrangement of the backbone made of sugars and phosphate groups joined by covalent ester bonds.[7,8] Attempts had been made to organize conductive chromophores along linear polymer chains[9–12] and in some cases the corresponding charge transport mobility was measured.[13] However, no enhancement of charge carrier mobility of such polymeric systems has been reported, compared to the corresponding monomer film. There remains a challenge to achieve the close intramolecular contact between the conductive units and to maximize the electronic coupling between them using covalent control. On the other hand, the organization of conductive units into two-dimensional covalent organic frameworks has been achieved.[14–16] The reported charge carrier mobilities, however, were from laser flash photolysis time-resolved microwave

[a]Department of Chemical Engineering, Stanford University, Stanford, CA 94305, USA. E-mail: zbao@stanford.edu

[b]Department of Chemistry and Biochemistry, University of California, Los Angeles, CA 90095, USA

[c]Division of Chemistry and Chemical Engineering, California Institute of Technology, Pasadena, CA 91125, USA

[d]Department of Chemistry & Chemical Biology, Harvard University, Cambridge, MA 02138, USA

[e]Department of Materials Science and Engineering, Stanford University, Stanford, CA 94305, USA

† Electronic supplementary information available. See DOI: 10.1039/c3tc31158a

conductivity measurements, on a scale of several nanometers that may not be applicable to micro-scale OFETs.

In order to investigate the effects of covalent local organization of conductive components on the optical and electronic properties, the polymer should have (i) high molecular weight (MW) in order to maximize the charge transport from intramolecular contribution, (ii) no structural and chemical defects in the repeating units, and (iii) a non-rigid backbone that ensures good solubility and allows the pendant groups to reorganize thermally for maximized intramolecular interactions. In addition to the better processability and thermal stability, for conductive polymers, a higher MW allows fewer hops between polymer chains and sometimes gives better connection between grains.[17,18] Good solubility is an essential property for solution-processed fabrication procedures. In this context, we designed (Fig. 1) a buckminsterfullerene (C_{60})-containing monomer terminated with a norbornene group for ring-opening metathesis polymerization (ROMP), leading to the corresponding brush-like polymer *via* a "graft through" route. However, according to a similar work reported in the literature,[19] the poor solubility of the C_{60} polymer will be a severe limiting factor to the MW. In this context, an essential solubilizing group, either polystyrene or branched alkyl chain, needs to be attached as the tail of the monomer. The polystyrene side-chain, in addition, provides the possibility of direct visualization of the single polymer chain under atomic force microscopy (AFM).[20,21]

C_{60} represents an ideal conductive component[22,23] for demonstrating that enhanced intramolecular charge transport can result in an overall increase in charge transport in the bulk thin film, based on the facts such as: (i) the isotropic spherical π-electron surface of C_{60} makes the charge transport insensitive to the precise C_{60} arrangements;[24,25] (ii) C_{60}-containing thin films are reported to have high electron mobility values;[4,26,27] and (iii) C_{60} units are bulky in size with a van der Waals diameter of ~1.1 nm so that they can easily interact with each other when in close proximity. The organization and assembly of fullerene units using non-covalent forces have been well documented in the literature.[28] We hypothesize that the one-dimensional covalent organization of C_{60} units along a linear polymer, in which the repeating unit is spatially smaller than the C_{60} unit, would confine them along the polymer chain with close contact (Fig. 1). Given the fact that the peculiar features of C_{60} are retained in most of its derivatives, such arrangements would promote intramolecular fullerene interactions, which could, in turn, result in fullerene-containing materials with improved charge transport.

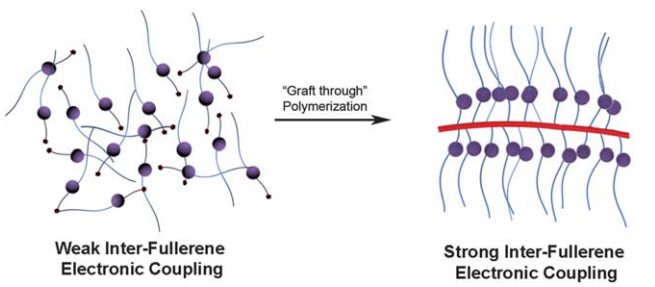

Fig. 1 Cartoon representation of the covalent organization of C_{60} units by the polymerization of a C_{60} containing monomer. The one-dimensionally organized C_{60} units should in principle exert stronger electronic coupling with each other, leading to improved intra-chain charge transport property compared to the monomer.

2 Result and discussion

2.1 Theoretical investigation of polymer design

In order to investigate the conformation of the proposed C_{60}-containing poly(norbornene) derivative and the packing mode of the C_{60} units, molecular dynamics (MD) simulations were performed on model molecules with 10 repeating units (structure shown in Fig. 2, top) in an explicit toluene solvent. The snapshots of configurations of polymers with three different lengths of spacers [$(CH_2)_m$, with $m = 3$, $m = 6$, and $m = 12$] obtained after 20 ns of simulations are shown in Fig. 2. The poly(norbornene) backbones are relatively rigid and remain nearly linear during the simulation period [the computed Debye–Waller factors (B-factors) of the backbones and side-chain C_{60} groups are provided in the ESI†]. 2-Decyltetradecanyl groups are flexible and may either interact with the C_{60} units or be exposed to the solvent, which leads to increased solubility. As we hypothesized, the distances between the C_{60} units on adjacent side-chains are dependent on the length of the spacer. For $m = 3$, the C_{60} units are aligned in a more linear arrangement and each C_{60} is in close proximity to the two adjacent C_{60} units on the side-chains. In contrast, when $m = 6$ or 12, the C_{60} units have more freedom of movement due to the longer spacer. In both cases, the fullerene units appeared to cluster on one side of the backbone, while on the other side the C_{60} units are separated into two groups. The histograms of the inter-fullerene distances are also shown in Fig. 2. For $m = 3$, most of the inter-fullerene distances are between 9 and 15 Å, while for $m = 6$ and 12, there are significant populations of the inter-fullerene distances between 15 and 25 Å. As a result, the average center-to-center distance between adjacent C_{60} units increases while increasing the length of alkyl spacers from $m = 3$ to $m = 6$ to $m = 12$ (10.98 ± 1.12, 11.49 ± 0.81 and 12.39 ± 1.27 Å, respectively). According to previous computational studies on fullerene–fullerene[29] (with the lowest energy inter-fullerene distance being 10.3 Å) and fullerene–π system[30] (with the π–π distance being 3.0 Å) interactions as well as crystallographic data on fullerenes in the solid state[31] (inter-fullerene distance 10.1 Å at room temperature), strong van der Waals interactions between the C_{60} units are expected at these distances.

In order to further investigate the effect of the confined local covalent organization on the charge transport properties in the polymers, we proceeded to perform quantum chemical calculations on the electronic coupling between the C_{60} units. To compare the magnitude of the transfer integrals for the polymer with $m = 3$ and $m = 12$, we have extracted 100 groups of two adjacent C_{60} units for snapshots taken every 200 fs from the 20 ns MD trajectories. The histograms for the absolute values of the transfer integrals are shown in Fig. 3. Higher transfer integral is

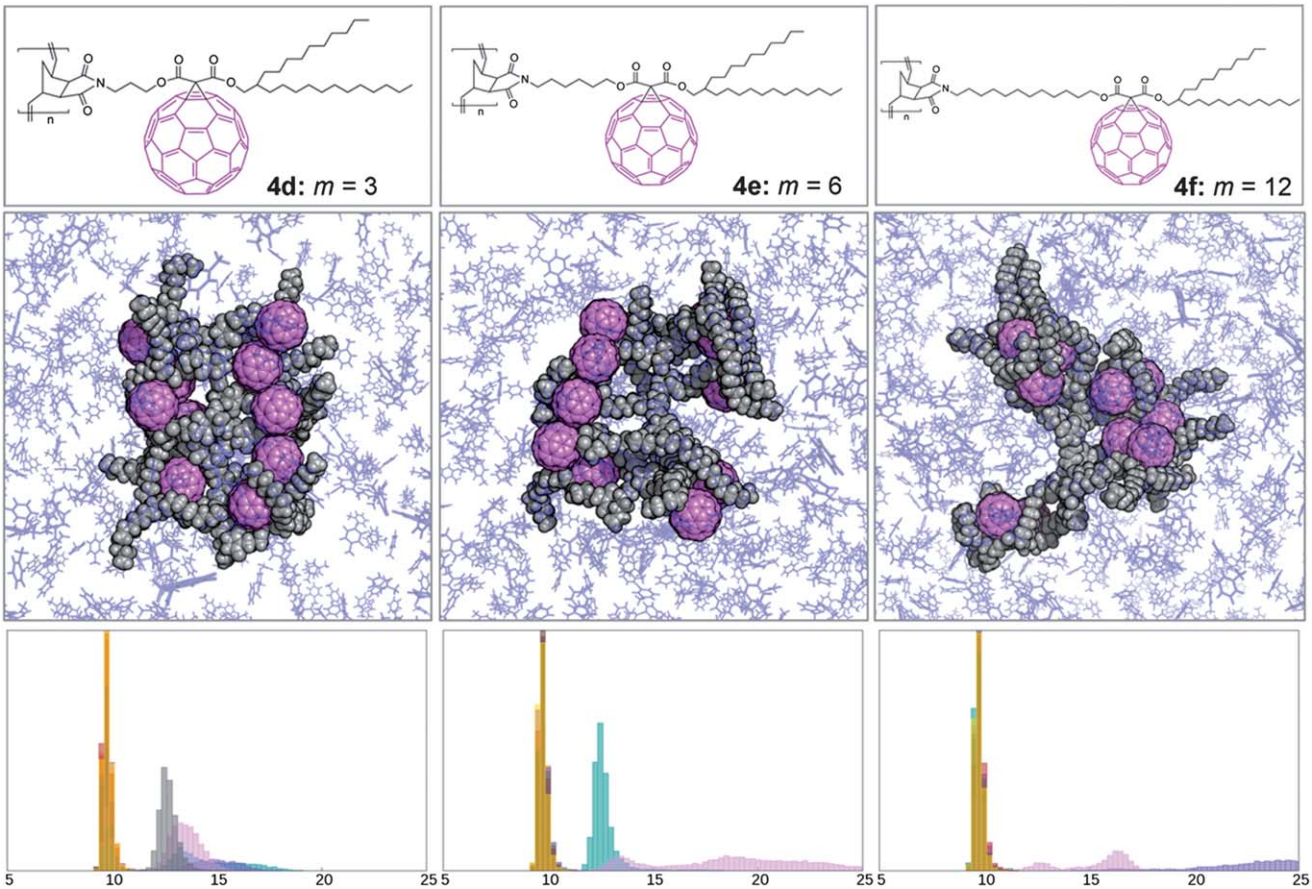

Fig. 2 (Top) Structural formula of the model molecules studied in the MD simulation, with different spaces $(CH_2)_m$ in between the poly(norbornene) backbones and the C_{60} units. (Middle) The snapshots of structures with $m = 3$, $m = 6$, and $m = 12$ after 20 ns of MD simulations in an explicit toluene solvent. (Bottom) The histogram of the distances between adjacent C_{60} units, calculated based on the centers of mass of each fullerene. Distances (in Å) between each pair of C_{60} units are shown in a unique color (see ESI† for the color code).

an indication of a better electronic coupling between molecules and therefore a faster charge transfer. When $m = 12$, most of the transfer integrals lied between 0 and 10 meV with a peak at the lower end. In contrast, the transfer integrals for $m = 3$ showed much broader distribution where most of the transfer integrals were between 10 and 20 meV. For the polymer with a shorter spacer, the transfer integrals also extended to higher values up to 50 meV with a lower count at around 0 meV. Such a drastic difference in transfer integrals demonstrates that the charge transfer among the side-chain C_{60} units is heavily governed by the confined covalent organization. A shorter spacer gives stronger coupling between adjacent C_{60} units and hence better charge transport characteristics in these side-chain polymers.

2.2 Synthesis and characterization

With the verification from MD simulation and quantum chemical calculation, we proceeded to the syntheses of spatially confined C_{60}-pendant poly(norbornene) derivatives. Fullerene-containing polymer materials[32] have been popular synthetic targets immediately after the successful production of C_{60} in a multi-gram scale.[22] Aside from a few examples of main-chain fullerene polymers reported[33–35] in the literature, many side-chain fullerene polymers were synthesized as pendant groups on non-conjugated[36–41] and conjugated polymer backbones.[42] Moreover, fullerene units were also incorporated successfully into cross-linked polymer matrices[43,44] and three-dimensional inorganic materials.[45] In spite of these synthetic achievements, most of the aforementioned polymers are limited in MW on account of the marginal solubility of fullerene in common organic solvents.[46] Furthermore, because of the significant spatial hindrance of the spherical C_{60} units, it is challenging to functionalize 100% of the side-chains with C_{60} units when using a "graft to" approach, inducing defects on the side-chains hence diminishing the intramolecular charge transport path. Instead, the "graft through" approach we adopted in this work enables 100% side chain occupation by C_{60} units, hence leading to a defect-free C_{60} polymer chain.

As outlined in Scheme 1, the synthesis started with the amination of *cis*-5-norbornene-*exo*-2,3-dicarboxylic anhydride by α,ω-amino alcohols **1a–c** with different carbon numbers m. Since the length of the amino alcohol determines the distance between the norbornene group and the fullerene unit, three different amino alcohols with the alkyl spacer carbon numbers $m = 3$, 6 and 12 were employed. The resulting hydroxyl group-terminated norbornene derivatives were subsequently treated

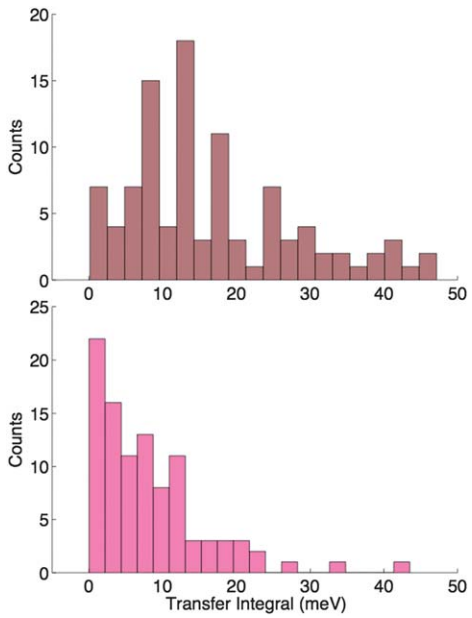

Fig. 3 Quantum chemistry calculation: calculated distribution of absolute values of the transfer integrals between a pair of C_{60} units in **4d** ($m = 3$, top) and **4f** ($m = 12$, bottom), based on the corresponding 20 ns molecular dynamics trajectories.

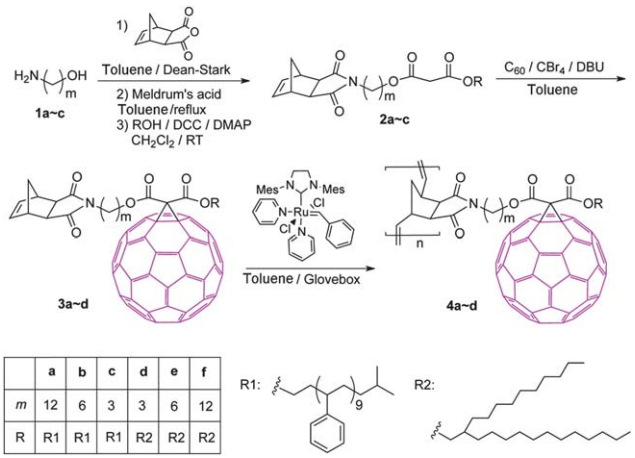

	a	b	c	d	e	f
m	12	6	3	3	6	12
R	R1	R1	R1	R2	R2	R2

Scheme 1 The synthetic scheme for the C_{60}-containing brush-like polymers **4a–d**. These polymers differ from each other in the spacer lengths (m) and the solubilizing groups (R), which are specified in the table box.

with Meldrum's acid to give the corresponding malonic acids. The solubilizing groups – either polystyrenes [$M_n = 900$ g mol^{-1}, polydispersity index (PDI) = 1.1] or branched alkyl chains – were attached by carbodiimide-promoted acid-alcohol coupling reactions to afford malonates **2a–f**. The resulting malonates can then undergo base-promoted Bingel cycloaddition[47] reactions with C_{60} to give the norbornene derived methanofullerenes **3a–f**. After extensive purification procedures, including column chromatography, preparative gel permeation chromatography (GPC) and re-precipitation, the pure **3a–f** were ready to undergo ROMP to give polymer products **4a–f**. In order to obtain high-MW products with controllable PDIs, the highly active fast-initiating ruthenium catalyst $(H_2IMes)(pyr)_2$-$(Cl)_2RuCHPh$[48] was

Table 1 Initiator ratio, molecular weight, polydispersity and TGA analysis of polymers **4a–f**

Entry	[M]/[I]	M_n (kg mol^{-1})	PDI	DP[c]	Theoretical C_{60} content (%)	Residual weight at 550 °C on TGA (%)
4a	800	1300[a]	1.9	1220	33.2	43.7
4b	800	770[a]	2.2	760	36.6	45.3
4c	400	370[a]	1.2	410	37.8	46.1
4d	400	160[b]	2.4	330	52.9	66.9
4f	400	249[b]	1.2	460	48.4	53.5

[a] Determined from GPC using THF as an eluent and polystyrene as the standards. [b] Determined from GPC using chlorobenzene as an eluent and polystyrene as the standard. [c] The size exclusion columns underestimated the MW of C_{60} containing polymers. In this context, the normalized DP values were calculated by dividing the GPC MW of the polymer by the GPC MW of the monomer, in order to minimize such underestimation on MW.

selected for the polymerization. Since the [Ru] catalyst loading was extremely low (<0.1% in weight) in the ROMP and was the only reagent introduced during the reaction, the polymer solutions were used as-prepared for characterization and device testing directly without further purification.

According to analytical GPC characterization (Table 1), the ROMP reactions proceeded quantitatively within 2 h. The products were clean with moderate polydispersity (PDI $\leq$ 2.4), and no monomer was detectable. The MWs of the products were controlled by the ratio of the monomer to the initiator ([M]/[I]) (Table 1). For example, the degree of polymerization (DP) of **4a** and **4b** was 1220 and 760, respectively, when using [M]/[I] = 800. In the case of **4c, d, and f**, [M]/[I] = 400 was used in the polymerization reaction, leading to DP = 410, 330, and 460 respectively (see ESI† for GPC and thermogravimetric analysis). The individual polymer chains were visualized directly in intermittent contact mode AFM (see ESI†). The high degree of polymerization rises the contour lengths of individual polymer chains up to several hundred nanometers while the long polystyrene side-chains ensured the rigidity and a significant height of the polymer chains when lying down on the surface.[21]

2.3 Optical spectroscopic characterization

In order to experimentally confirm the interaction between C_{60} molecules in polymers with different spacer lengths, we carried out optical spectroscopic characterizations. When closely packed to each other, fullerene molecules undergo intermolecular charge transfer (CT) with their nearest neighbor. Such CT interactions result[24] in new absorption bands, centered around 510 nm and 460 nm. They are, for example, present in the thin films of [6,6]-phenyl-C_{61}-butyric acid methyl ester (PCBM), but are suppressed when PCBM is diluted in a polymer matrix.[49] In this context, solution UV/vis absorption spectra (Fig. 4a) of polymers **4a–c** (with m = 12, 6 and 3, respectively) and monomer **3a** were recorded. In order to probe only intramolecular interactions, dilute solutions (0.2 mg mL^{-1}) in toluene were employed for the solution experiments. The solution UV/vis spectrum of monomer **3a** showed a sharp peak

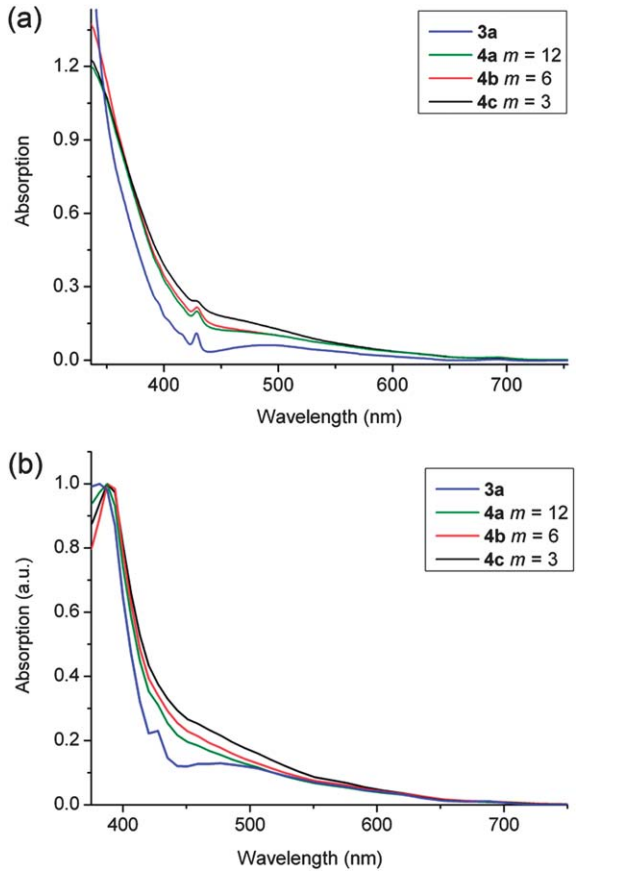

Fig. 4 (a) UV/vis spectra of **4a–c** and **3a** recorded in solutions (0.2 mg mL^{-1}) in toluene. (b) Photothermal deflection spectra of **4a–c** and **3a** in thin films that were drop-cast onto quartz substrates (2% in polystyrene matrix).

at 430 nm and a broad peak maximized at 490 nm, with two distinctive dips on absorption (425 and 435 nm) before and after the peak at 430 nm. These characteristic absorption features represent free methanofullerene derivatives in solution, similar to those reported for PCBM.[50] The spectrum of **4a** ($m = 12$), however, showed the same absorption features but the absorbance from 400 to 550 nm increased, making the peak at 430 nm less sharp compared to that of **3a**. For **4b**, a shorter spacer ($m = 6$) made the peak at 430 nm even broader. When **4c** ($m = 3$) was measured, such a trend was most prominent and the peak at 430 nm was almost indistinguishable, making the spectrum of **4c** to resemble that of a thin-film of the C_{60} derivative, even though this case is for a dilute solution.[49,51] Moreover, cyclic voltammetry measurement of the dilution solution of the polymer showed a ~50 mV increase in the electron affinity compared to the corresponding monomer, corroborating[52] the fact that the C_{60} units were in close contact with each other along the polymer chain (see ESI†).

In order to test whether such a phenomenon retains in the solid state, the absorption spectra of the thin films of **4a–c** (2% by weight) dispersed in the polystyrene matrix were recorded (Fig. 4b). Photothermal deflection spectroscopy[53] (PDS) was employed to rule out any influence of light scattering on the solid-state optical absorption spectrum in the spectral region of interest, as PDS is a technique insensitive to light scattering. It was observed that the absorption increased in the spectral region between 450 nm and 550 nm for the polymers, with the same trend compared to solution UV/vis spectra, *i.e.*, the polymers with shorter spacer lengths exhibit stronger CT absorption, consistent with the shorter inter-fullerene distance in the MD simulations. Considering the low concentration of the polymer/monomer, we attribute such a trend to the increasing probability of intramolecular C_{60}–C_{60} interactions along the polymer chain while decreasing the spacer length m, suggested by the MD calculations described earlier.

Although a number of examples of the synthesis and characterization of brush-type fullerene polymers have been reported[29–33] in the literature, they did not demonstrate the property of confined assembly of the fullerene units. The conventional "graft to" synthetic approach, in which side-chain defects are inevitable due to the increasing steric blocking of the grafting site as the reaction proceeds, limits the possibility of close interaction between the side-chain fullerene units. This challenge was overcome herein by using the "graft through" approach using a fullerene-containing monomer, to force a 100% occupation of C_{60} units on the side-chains even though the resulting steric hindrance of the side-chains is significant.

2.4 Thin film processing and field-effect transistors

To investigate the solid-state electronic properties of the confined organized C_{60} units along the polymer chains, charge carrier mobility of the thin films formed by the polymers and the corresponding monomers was measured. Smooth thin-films of the monomers **3a–f** and the polymers **4a–f** can be readily formed on hydrophobic substrates by spin-casting. Both the thin films of the polymers and the monomers were smooth and amorphous. For example, the mean roughness of a thin-film of **4d** was measured by AFM to be 0.28 nm and that of its monomer **3d** was 0.24 nm. Grazing incidence X-ray diffraction (GIXD) of the thin films of **3d** and **4d** demonstrated that both the films are amorphous without any identifiable crystalline domain (see AFM and GIXD data in ESI†). It is noteworthy that if the polymers **4a–f** were precipitated out in a poor solvent such as MeOH, the resulting solid cannot be re-dissolved in good solvents. This phenomenon is likely a result of an extremely slow dissolving process of the large C_{60}-containing polymers, even though the original solutions of **4a–f** are thermodynamically stable.[54] Such a unique property is essential for sequential solution-processed techniques because one can cast a thin film on top of the solvent-resistant film without re-dissolving the formerly casted thin-film.[55] Indeed, immersing the thin-film of **4a–f** covered substrates in solvents such as toluene, THF and *o*-DCB for 24 h neither dissolve the polymer thin-film nor change the surface morphology.

Polymer **4d, f** and their monomeric precursor **3d, f** were chosen for the fabrication of thin-film transistors (TFT), because of their highest C_{60} contents among **3a–f** and **4a–f**.[56] Fig. 5 displays transfer (I_{DS} *vs.* V_{GS}) characteristics of OFETs based on **4d, f** and **3d, f** annealed at 100 °C under nitrogen for 1 h, and the typical output (I_{DS} *vs.* V_{DS}) of device **4d** at different

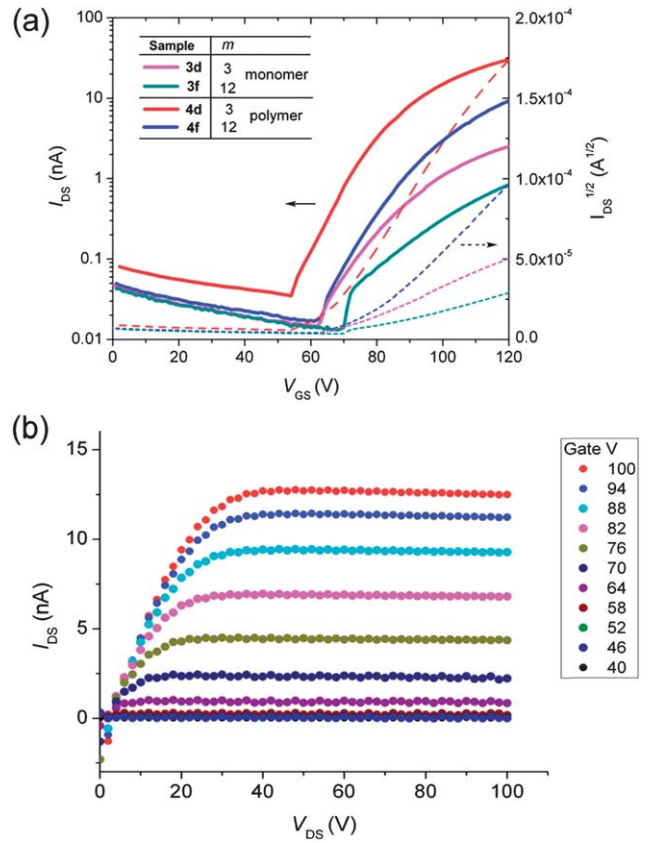

Fig. 5 (a) Transfer character of the OFET of **3d** and **3f** (monomers) as well as **4d** and **4f** (polymers) as spin-cast thin films on BCB (10 nm) coated SiO_2 (300 nm)/Si substrates, with $V_{DS} = 120$ V; (b) output of the OFET of **4d**.

gate voltages. As shown in Fig. 5 and Table 2, both the polymers and the monomers demonstrated characteristic *n*-type field-effects. In N_2, the mobility of monomers **3d** and **3f** was measured to be 6.8×10^{-6} and 3.2×10^{-6} cm^2 V^{-1} s^{-1}, respectively. The mobility of the polymers, **4d** and **4f**, was measured to be more than an order of magnitude higher (1.1×10^{-4} and 5.8×10^{-5} cm^2 V^{-1} s^{-1}, respectively).

Although the mobilities of these materials were much lower compared to those of C_{60} derivatives such as PCBM, attributed to the lower C_{60} content (48–53%), the TFT of **4d, f** did exhibit a higher field-effect compared to that of monomers **3d, f.** Not only was the electron mobility higher by more than an order of magnitude, but also the on/off ratio was significantly larger. Considering that the constitutional structures of the monomers and their polymeric counterparts are highly analogous and the micro-morphologies of the thin films were both smooth and amorphous, we attribute the difference in mobility to the confined organization of C_{60} units in **4d, f**, and possibly a higher chance of interstrand charge hopping due to an increased possibility of contacting between polymers, compared to the corresponding monomers **3d, f.** The confined arrangement of C_{60} units along the long polymer chain in the thin films of **4d** and **4f** facilitated intra-polymer chain electron transport, while such an advantage is not available in the thin films of **3d** and **3f.** Moreover, a higher charge carrier mobility was observed for **4d** with a shorter spacer than that of **4f** with a longer spacer, in agreement with the quantum chemical calculation results that the intramolecular transfer integral in **4d** is higher than that in **4f.** The difference in mobility of **4d** and **4f** also indicated that the improved intrachain charge transport was a dominant factor for the improvement of charge transport in the polymers, compared to the factor of improved interstrand charge hopping between the polymer chains. However, in the long range at a scale of the device channel length (~50 μm), the barriers for charge carrier hopping between polymer chains in the thin film of the polymers were still the main limiting effect for the charges to transport, restricted the enhancement of electron mobility by having the intramolecular local confined arrangement of conductive C_{60} units.

As mentioned earlier, the as-prepared polymer solution can be used to cast thin films right after the polymerization is completed; the thin films become insoluble once dried. In order to test the stability of the solvent resistant thin film, the TFT device of **4d** was tested in air, before and after soaking it in toluene, giving average electron mobilities of 8.5×10^{-5} and 3.8×10^{-5} cm^2 V^{-1} s^{-1} (see ESI†). The mobility decreased only slightly even after soaking in toluene for 24 h. The retention of the electron transport ability of **4d** makes these polymers interesting for solution-processing of solar cells or doped conductors that require solvent resistance.[55] For example, they could serve as the interface layer in solution-processed solar cells. Because of their excellent solvent resistance and highly amorphous morphology, such polymer thin films allow layer-by-layer processing on top of them without the issue of re-dissolving. Meanwhile, as a very thin interface layer, the moderate mobility should be sufficient to accommodate the current density of organic solar cells.

Table 2 Average mobility, on/off ratio, and threshold voltage for the OTFT devices fabricated using **3d/f** and **4d/f**, measured in N_2. All the devices were measured right after each other on the same day within a few hours, with the same solution-processing technique, and the same annealing process. Each of the compounds had been tested on devices from at least two different batches, and on 5 different channels of each batch. The results were within their standard deviation listed below

Samples	Mobility (cm^2 V^{-1} s^{-1})	On/off	V_t
3d	$(6.8 \pm 2.2) \times 10^{-6}$	160	63 ± 2
4d	$(1.1 \pm 0.2) \times 10^{-4}$	770	63 ± 1
3f	$(3.2 \pm 1.0) \times 10^{-6}$	70	60 ± 3
4f	$(5.8 \pm 1.7) \times 10^{-5}$	650	79 ± 4

3 Conclusion

In summary, the synthesis of high polymers with close packing of C_{60} side-chains was achieved by using the highly efficient [Ru] catalyzed ROMP reactions. Experiments and molecular dynamics calculations demonstrated that the fullerene units were confined along the polymer backbone and were forced to interact with one another. The length of the spacer linking the C_{60} unit and the poly(norbornene) backbone can be tuned, in order to govern the inter-fullerene interactions: a longer spacer gives more space for the side chain to relax so that the C_{60} units

can keep distance from each other; a shorter spacer forces the C_{60} unit to be attached closely to the main chain, increasing the inter-fullerene interactions. Such intramolecular C_{60} interactions enhanced the corresponding electronic coupling, calculated by quantum chemistry methods. The measured electron mobility of the polymer thin-films was found to be more than an order of magnitude higher than that of the corresponding monomer. This work demonstrates improved charge transport in a bulk organic material through enhanced intramolecular charge transport by means of one-dimensional covalent organization. Because the inter-chromophore distance as well as the degree and phase of π-overlapping are the key parameters in determining the charge transport mechanism of organic semiconductors (the newly suggested "band-like" charge transport *vs.* the classical charge hopping mechanism[57,58]), the ability to control these parameters using covalent bonds provides an important method to study these mechanisms systematically. This design strategy for the regulation of electronic behavior of organic conductive components would also apply to non-fullerene systems.[10,13] It can also be further coupled with the strategy of side-chain tuning, which helps to decrease the interchain transport, to capitalize the overall enhancement of charge transport in bulk. Moreover, these polymer thin films showed excellent solvent resistance as a result of their high molecular weight despite their high solubility, making them potentially interesting in solution-processed device fabrications.

4 Experimental

Molecular dynamics simulations

Molecular dynamics simulations were performed using AMBER 11 (ref. 59) and the general AMBER force field (GAFF)[60,61] for polymers with three different lengths of spacers, $m = 3$ (**4d**), $m = 6$ (**4e**), and $m = 12$ (**4f**). The 2-decyl-tetradecanyl solubilizing group, which is less computationally demanding than the polystyrene side chain, was used in the simulations for all polymers. The starting structure was constructed with a *trans*-isotactic backbone with 10 repeating monomers for each polymer, five on each side of the backbone. The distance between the centers of adjacent C_{60} is 9.54 Å (with a surface–surface distance of 2.4 Å) in the starting geometry. (For references and details regarding the computational methods, see ESI.†)

Synthesis of polymers 4a–f

In a glovebox, the [Ru] catalyst was dissolved in degassed toluene in a vial to make a catalyst stock solution (1 mg mL^{-1}). **3a–f** were also dissolved in degassed toluene to make a reaction solution (30 mg mL^{-1}) in a vial using a magnetic stirring bar. To the reaction solution was added the corresponding amount of catalyst solution while stirring. The reaction was allowed to proceed for 2 h before being transferred out of the glovebox. The mixture was stirred open to the air for another 30 min and then sealed for storage.

Atomic force microscopy

AFM images were taken on a Multimode atomic force microscope (Veeco). By spin-coating (5000 rpm) a diluted solution of **4b** or **4c** (0.01 mg mL^{-1}) in 1,2-dichlorobenzene onto a freshly split mica substrate, the polymer can be deposited onto the surface without severe aggregation and the individual polymer chain can be identified in intermittent contact mode (light tapping regime).

Photothermal deflection spectroscopy

4a–c or **3a** and polystyrene (MW = 40 kg mol^{-1}) were dissolved in toluene at a ratio of 1 : 50 to form a blend solution (10 mg mL^{-1}). The thin film samples for PDS measurement were prepared by drop casting these solutions onto quartz substrates. PDS measures the local heating of the sample caused by the absorption of monochromatic light and subsequent non-radiative decay. For weakly absorbing samples the PDS-signal is proportional to the absorption coefficient of the material and provides a scatter free method of measuring its wavelength dependence.

In our home-built setup, the light of a Xe lamp passes through a Newport Oriel cornerstone 260¼ m monochromator and is focused onto the sample. The light beam (pump) is chopped at a frequency of 3.333 Hz, creating a periodic heating, causing a thermal wave to propagate in the sample and into the surrounding medium. The sample is immersed in perfluorohexane (C_6F_{14}, 3M Fluorinert FC-72), which has a strongly temperature dependent index of refraction. This index of refraction change is probed by a HeNe laser (633 nm), of which the deflection is detected by a position sensitive Si detector connected to a Stanford research system SR830 lock-in amplifier. At the same time, the intensity of the incident monochromatic pump beam is measured by a pyroelectric detector connected to a second lock-in amplifier. Dividing the two signals from the lock-ins yields the PDS absorption spectrum.

Quantum chemistry calculations

The transfer integrals for the LUMO orbitals were calculated within the dimer approximation at the B3LYP/6-31G(d) level of theory as implemented in the Q-Chem 3.2 quantum chemistry package. Although the 6-31G(d) basis is known to underestimate the strength of the couplings, it has been shown that the qualitatively correct results were obtained at this level of theory. The solubilizing groups and the spacers to the polymer backbone are replaced by *methyl* groups to reduce the size of the system. (See ESI† for references and the detailed structure used for the calculations.)

Thin film transistors

The SiO_2 dielectric surface (300 nm thick) of a heavily n-doped silicon wafer was covered with a 10 nm thick film of a cross-linked bisbenzocyclobutene (BCB) layer. A thin film of **3d, 3f, 4d** or **4f** was deposited on top of the BCB treated substrate by spin-coating a polymer solution in toluene (10 mg mL^{-1}) at 1000 rpm for 60 s. The film thicknesses were all within the range of 44 ± 2 nm. Au source/drain electrodes ($W = 1000$ μm, $L = 50$ μm) were used to measure the electrical performance. The average field-effect mobilities were calculated from the transfer characteristics of more than 5 devices in the saturation region ($V_{DS} = 100$–120 V).

Acknowledgements

We are grateful to the National Science Foundation (Z. B.: DMR-1006989; K. N. H.: CHE-1059084; A. A.-G.: DMR-08-20484) and Defense Advanced Research Projects Agency (Z. B. & A. A.-G.: QuBE) for financial support of this research. We are also grateful to the Stanford GCEP initiative (A. A.-G, S. S. and S. A.). S. O. acknowledges the European Community for the post-doctoral fellowship PIOF-GA-2009-252856. G. J.-O. acknowledges the Ministerio de Educación for the postdoctoral fellowship EX2010-1063. We thank the High Performance Technical Computing Center at the Faculty of Arts and Sciences of Harvard University for invaluable support.

References

1 M. Mas-Torrent and C. Rovira, *Chem. Rev.*, 2011, **111**, 4833–4856.
2 H. Moon, R. Zeis, E.-J. Borkent, C. Besnard, A. J. Lovinger, T. Siegrist, C. Kloc and Z. Bao, *J. Am. Chem. Soc.*, 2004, **126**, 15322–15323.
3 M. Gsanger, J. H. Oh, M. Konemann, H. W. Hoffken, A. M. Krause, Z. N. Bao and F. Würthner, *Angew. Chem., Int. Ed.*, 2010, **49**, 740–743.
4 H. Li, B. C. K. Tee, J. J. Cha, Y. Cui, J. W. Chung, S. Y. Lee and Z. Bao, *J. Am. Chem. Soc.*, 2012, **134**, 2760–2765.
5 J. A. Merlo and C. D. Frisbie, *J. Phys. Chem. B*, 2004, **108**, 19169–19179.
6 S. Fabiano, H. Wang, C. Piliego, C. Jaye, D. A. Fischer, Z. Chen, B. Pignataro, A. Facchetti, Y.-L. Loo and M. A. Loi, *Adv. Funct. Mater.*, 2011, **21**, 4479–4486.
7 J. C. Genereux and J. K. Barton, *Chem. Rev.*, 2009, **110**, 1642–1662.
8 J. D. Slinker, N. B. Muren, S. E. Renfrew and J. K. Barton, *Nat. Chem.*, 2011, **3**, 228–233.
9 P. A. J. de Witte, M. Castriciano, J. J. L. M. Cornelissen, L. Monsù Scolaro, R. J. M. Nolte and A. E. Rowan, *Chem.–Eur. J.*, 2003, **9**, 1775–1781.
10 O. Y. Kas, M. B. Charati, L. J. Rothberg, M. E. Galvin and K. L. Kiick, *J. Mater. Chem.*, 2008, **18**, 3847–3854.
11 C.-M. Chou, S.-L. Lee, C.-H. Chen, A. T. Biju, H.-W. Wang, Y.-L. Wu, G.-F. Zhang, K.-W. Yang, T.-S. Lim, M.-J. Huang, P.-Y. Tsai, K.-C. Lin, S.-L. Huang, C.-h. Chen and T.-Y. Luh, *J. Am. Chem. Soc.*, 2009, **131**, 12579–12585.
12 Y. Zheng, J. Cui, J. Zheng and X. Wan, *J. Mater. Chem.*, 2010, **20**, 5915–5922.
13 C. E. Finlayson, R. H. Friend, M. B. J. Otten, E. Schwartz, J. Cornelissen, R. L. M. Nolte, A. E. Rowan, P. Samori, V. Palermo, A. Liscio, K. Peneva, K. Mullen, S. Trapani and D. Beljonne, *Adv. Funct. Mater.*, 2008, **18**, 3947–3955.
14 X. Ding, L. Chen, Y. Honsho, X. Feng, O. Saenpawang, J. Guo, A. Saeki, S. Seki, S. Irle, S. Nagase, V. Parasuk and D. Jiang, *J. Am. Chem. Soc.*, 2011, **133**, 14510–14513.
15 S. Wan, F. Gandara, A. Asano, H. Furukawa, A. Saeki, S. K. Dey, L. Liao, M. W. Ambrogio, Y. Y. Botros, X. Duan, S. Seki, J. F. Stoddart and O. M. Yaghi, *Chem. Mater.*, 2011, **23**, 4094–4097.
16 X. Feng, L. L. Liu, Y. Honsho, A. Saeki, S. Seki, S. Irle, Y. P. Dong, A. Nagai and D. L. Jiang, *Angew. Chem., Int. Ed.*, 2012, **51**, 2618–2622.
17 J. Kline, M. D. McGehee, E. N. Kadnikova, J. Liu and J. M. J. Frechet, *Adv. Mater.*, 2003, **15**, 1519–1522.
18 H. N. Tsao, D. M. Cho, I. Park, M. R. Hansen, A. Mavrinskiy, D. Y. Yoon, R. Graf, W. Pisula, H. W. Spiess and K. Mullen, *J. Am. Chem. Soc.*, 2011, **133**, 2605–2612.
19 Z. T. Ball, K. Sivula and J. M. J. Fréchet, *Macromolecules*, 2006, **39**, 70–72.
20 S. S. Sheiko and M. Moller, *Chem. Rev.*, 2001, **101**, 4099–4123.
21 Y. Xia, A. J. Boydston and R. H. Grubbs, *Angew. Chem., Int. Ed.*, 2011, **50**, 5882–5885.
22 W. Kratschmer, L. D. Lamb, K. Fostiropoulos and D. R. Huffman, *Nature*, 1990, **347**, 354–358.
23 F. Wudl, *J. Mater. Chem.*, 2002, **12**, 1959–1963.
24 S. Kazaoui, N. Minami, Y. Tanabe, H. J. Byrne, A. Eilmes and P. Petelenz, *Phys. Rev. B: Condens. Matter Mater. Phys.*, 1998, **58**, 7689–7700.
25 H. Tamura and M. Tsukada, *Phys. Rev. B: Condens. Matter Mater. Phys.*, 2012, **85**, 054301.
26 T. D. Anthopoulos, B. Singh, N. Marjanovic, N. S. Sariciftci, A. M. Ramil, H. Sitter, M. Colle and D. M. de Leeuw, *Appl. Phys. Lett.*, 2006, **89**, 213504.
27 X. H. Zhang and B. Kippelen, *Appl. Phys. Lett.*, 2008, **93**, 133305.
28 C.-C. Chu, G. Raffy, D. Ray, A. D. Guerzo, B. Kauffmann, G. Wantz, L. Hirsch and D. M. Bassani, *J. Am. Chem. Soc.*, 2010, **132**, 12717–12723.
29 J. M. Pacheco and J. P. P. Ramalho, *Phys. Rev. Lett.*, 1997, **79**, 3873–3876.
30 Y. Zhao and D. G. Truhlar, *Phys. Chem. Chem. Phys.*, 2008, **10**, 2813–2818.
31 D. L. Dorset and M. P. McCourt, *Acta Crystallogr., Sect. A: Found. Crystallogr.*, 1994, **50**, 344–351.
32 N. Martín and F. Giacalone, *Fullerene Polymers: Synthesis, Properties and Applications*, Wiley-VCH Verlag GmbH & Co. KGaA, Weinheim, Germany, 2009.
33 M. Taki, S. Takigami, Y. Watanabe, Y. Nakamura and J. Nishimura, *Polym. J.*, 1997, **29**, 1020–1022.
34 S. Samal, B. J. Choi and K. E. Geckeler, *Chem. Commun.*, 2000, 1373–1374.
35 R. C. Hiorns, E. Cloutet, E. Ibarboure, L. Vignau, N. Lemaitre, S. Guillerez, C. Absalon and H. Cramail, *Macromolecules*, 2009, **42**, 3549–3558.
36 S. Shi, K. C. Khemani, Q. C. Li and F. Wudl, *J. Am. Chem. Soc.*, 1992, **114**, 10656–10657.
37 Y. P. Sun, G. E. Lawson, W. J. Huang, A. D. Wright and D. K. Moton, *Macromolecules*, 1999, **32**, 8747–8752.
38 U. Stalmach, B. de Boer, C. Videlot, P. F. van Hutten and G. Hadziioannou, *J. Am. Chem. Soc.*, 2000, **122**, 5464–5472.
39 S. Ohsawa, K. Maeda and E. Yashima, *Macromolecules*, 2007, **40**, 9244–9251.
40 J. Kim, M. H. Yun, J. Lee, J. Y. Kim, F. Wudl and C. Yang, *Chem. Commun.*, 2011, **47**, 3078–3080.
41 M. Eo, S. Lee, M. H. Park, M. H. Lee, S. Yoo and Y. Do, *Macromol. Rapid Commun.*, 2012, **33**, 1119–1125.

42 T. Benincori, E. Brenna, F. Sannicolo, L. Trimarco, G. Zotti and P. Sozzani, *Angew. Chem., Int. Ed.*, 1996, **35**, 648–651.
43 T. Haino, E. Hirai, Y. Fujiwara and K. Kashihara, *Angew. Chem., Int. Ed.*, 2010, **49**, 7899–7903.
44 C.-H. Hsieh, Y.-J. Cheng, P.-J. Li, C.-H. Chen, M. Dubosc, R.-M. Liang and C.-S. Hsu, *J. Am. Chem. Soc.*, 2010, **132**, 4887–4893.
45 W. Whitnall, L. Cademartiri and G. A. Ozin, *J. Am. Chem. Soc.*, 2007, **129**, 15644–15649.
46 R. S. Ruoff, D. S. Tse, R. Malhotra and D. C. Lorents, *J. Phys. Chem.*, 1993, **97**, 3379–3383.
47 C. Bingel, *Chem. Ber./Recl.*, 1993, **126**, 1957–1959.
48 T. L. Choi and R. H. Grubbs, *Angew. Chem., Int. Ed.*, 2003, **42**, 1743–1746.
49 S. Cook, H. Ohkita, Y. Kim, J. J. Benson-Smith, D. D. C. Bradley and J. R. Durrant, *Chem. Phys. Lett.*, 2007, **445**, 276–280.
50 J. A. Mikroyannidis, A. N. Kabanakis, S. S. Sharma and G. D. Sharma, *Adv. Funct. Mater.*, 2011, **21**, 746–755.
51 The optical band gaps for the C_{60} monomer and polymers were not affected by the inter-fullerene interactions. Based on the onsets of the absorption spectra in solution and PDS spectra in the solid-state (Fig. 4), the band gaps of **3a** and **4a–c** were all calculated to be around 1.7 eV.
52 F. C. Jamieson, E. B. Domingo, T. McCarthy-Ward, M. Heeney, N. Stingelin and J. R. Durrant, *Chem. Sci.*, 2012, **3**, 485–492.
53 W. B. Jackson, N. M. Amer, A. C. Boccara and D. Fournier, *Appl. Opt.*, 1981, **20**, 1333–1344.
54 No precipitate can be observed after storing **4a–d** as 30 mg mL^{-1} solutions at room temperature in the dark for six months.
55 H. J. Kim, A. R. Han, C.-H. Cho, H. Kang, H.-H. Cho, M. Y. Lee, J. M. J. Fréchet, J. H. Oh and B. J. Kim, *Chem. Mater.*, 2011, **24**, 215–221.
56 The thin films of **4a–c** exerted marginal field-effects on account of their low contents of C_{60} and high contents of polystyrene side chains. The polystyerene chains could serve as thick insulating sheaths around the conductive C_{60} core, making the intermolecular charge transport unfavourable.
57 T. Sakanoue and H. Sirringhaus, *Nat. Mater.*, 2010, **9**, 736–740.
58 A. Troisi, *Org. Electron.*, 2011, **12**, 1988–1991.
59 D. A. Case, T. A. Darden, T. E. Cheatham, C. L. Simmerling, J. Wang, R. E. Duke, R. Luo, M. Crowley, R. C. Walker, W. Zhang, K. M. Merz, B. Wang, S. Hayik, A. Roitberg, G. Seabra, I. Kolossváry, K. F. Wong, F. Paesani, J. Vanicek, X. Wu, S. R. Brozell, T. Steinbrecher, H. Gohlke, L. Yang, C. Tan, J. Mongan, V. Hornak, G. Cui, D. H. Mathews, M. G. Seetin, C. Sagui, V. Babin and P. A. Kollman, *AMBER 11*, University of California, San Francisco, 2011.
60 J. M. Wang, R. M. Wolf, J. W. Caldwell, P. A. Kollman and D. A. Case, *J. Comput. Chem.*, 2004, **25**, 1157–1174.
61 G. Su, A. Czader, D. Homouz, G. Bernardes, S. Mateen and M. S. Cheung, *J. Phys. Chem. B*, 2012, **116**, 8460–8473.